Blasch, G., Spengler, D., Hohmann, C., Neumann, C., Itzerott, S., Kaufmann, H. (2015): Multitemporal soil pattern analysis with multispectral remote sensing data at the field-scale. - *Computers and Electronics in Agriculture*, *113*, p. 1-13.

DOI: http://doi.org/10.1016/j.compag.2015.01.012

Multitemporal soil pattern analysis with multispectral remote sensing data at the field-scale

Gerald Blasch[1]*, Daniel Spengler[1], Christian Hohmann[1], Carsten Neumann[1], Sibylle Itzerott[1], Herrmann Kaufmann[1]

[1] *GFZ German Research Centre for Geosciences Potsdam, Geodesy & Remote Sensing*

* *Corresponding author: Tel.: +49-331-2881187; fax: +49-331-2881192; E-mail: gerald.blasch@gfz-potsdam.de.*

Abstract

This research proposes a new model for the generation of basic soil information maps for precision agriculture based on multitemporal remote sensing data analysis and GIS spatial data modelling. It demonstrates (i) the potential of multitemporal soil pattern analysis (ii) to generate functional soil maps at field scale based on soil reflectance patterns and related soil properties and (iii) how to improve these soil maps based on the identification of static homogenous soil patterns by excluding temporal influences from the developed prediction model. Principal components and per-pixel analyses are used for the separation of static soil pattern from temporal reflectance pattern, influenced by (vital and senescent) vegetation and land management practices. The potential of the proposed algorithm is investigated using multitemporal multispectral RapidEye satellite imagery at a demonstration field "Borrentin" field in Northeast Germany.

Keywords: Precision agriculture; site-specific management; remote sensing; GIS; multitemporal; soil pattern; spatiotemporal variability; bare soil; organic matter;

1 Introduction

Soil maps provide basic knowledge regarding soil-landform interactions and soil variability across diverse landscapes (Zhu et al. 2013). Qualitative and quantitative soil data at different scales (landscape- or field-scale) are increasingly desired for (1) general policy-making, land resource management and environmental monitoring and (2) more precise applications in precision agriculture, hydrological modelling and soil landscape studies (Franzen et al. 2002; Lin et al. 2005a; Lin et al. 2005b; Robert 1993).

The concept of precision agriculture is based on the presence of temporal and spatial within-field variability of soil and crop characteristics (Zhang et al. 2002). Precision agriculture responds to this variability with fine-scale information-based optimization of farm inputs (e.g., fertiliser, herbicides, and seeds) to increase farm profitability, crop productivity, environmental quality and sustainability (Ge et al. 2011; Mulla 2013). The nucleus of site-specific management (SSM), a common precision agriculture practice, is the identification of (crop) management zones as "relatively homogenous sub-units of farm fields that can each be managed with a different, but uniform, customised management practice" (Mulla 2013). Management zones usually reflect within-field variability at scales finer than soil mapping units in the form of soil pattern or vegetation pattern. Addressing site-specific variability requires more specific information regarding the soil properties (i.e., mapped on functional soil maps)

than can be offered by traditional soil maps based on conceptual generalization-models of remotely sensed data, direct field survey, and special knowledge of soil, terrain, geology, vegetation and human factors (Zhu et al. 2013).

In recent years, numerous quantitative soil mapping models and approaches for the determination of soil properties at the field-scale based on DEM, proximal and/or remote sensing data have been developed. Spatial and geostatistical techniques, such as inverse distance calculations, various kriging-procedures, fuzzy clustering algorithms (Birrell et. al. 1996; Gotway et al. 1996; Guo et al. 2013; Liu et al. 2008; López-Granados et al. 2005; Sumfleth and Duttmann 2007; Triantafilis et al. 2009; Yan et al. 2007; Zhu et al. 2013), can transfer punctual quantitative soil property data to fine-scale soil maps, depending on the sampling strategy and the accuracy of the extensive, time-consuming and costly field survey. Non-invasive proximal and remote sensors and their corresponding physical-based or empirical-based data analysis methods have been approved as potentially effective, rapid and cost efficient (Mulder et al. 2011) and provide continuous, direct or indirect data on physiochemical soil properties depending on spatial, temporal or spectral sensor resolution. Several studies have analysed the relationships between soil reflectance characteristics, such as soil colour and soil brightness/lightness, and soil properties (Hummel et al. 2001; Viscarra Rossel et al. 2006; Viscarra Rossel et al. 2009; Singh et al. 2004; Spielvogel et al. 2004).

Ge et al. (2011), Mulla (2013), Plant (2001), Panda et al. (2010) and Zhang et al. (2002) offer a research overview of proximal sensing systems (e.g., spectroscopy, soil electrical conductivity sensors, and NIR-sensors) and remote sensing systems (e.g., multi- and hyperspectral satellite sensors and LIDAR based DEMs), as well as their applications in agriculture and soil science, including crop yield, biomass, crop nutrients, water stress, infestations of weeds, insects and plant diseases, hail or wind damage and especially soil properties (e.g., organic matter, moisture, texture, pH, nitrogen, salinity, and cation exchange capacity).

Although quantitative information regarding soil properties could not be measured directly using qualitative multispectral data methods (e.g., colour composites, band ratios, indices, and transformations), there are several advantages to the use of multispectral (low-spectral-resolution) data for SSM applications: (1) very high return frequency, (2) spatial resolution, (3) existing data archives, (4) relatively low costs and (5) accessibility. The cause of high-temporal and high-spatial resolution multispectral imagery and time-series are suited for information extraction of qualitative determinations, delineation of management zones, deriving soil patterns and determining and mapping soil surface units (Ge et al. 2011; Mulder et al. 2011).

Sommer et al. (2003) remarked that in addition to technical and methodical progress, a deeper understanding of temporal-spatial variability and soil pattern properties as well as the underlying development processes is still highly demanded, especially for choosing best-SSM practices. McBratney (2000; 2003) reviewed various hybrid approaches of quantitative soil pattern analysis.

For precision agriculture application in Germany, Lamp et al. (2001; 2002) presented the concept of “Digitale Hofbodenkarte” as a data fusion model based on field surveys, existing soil maps (e.g. Bodenschätzung 1:10.000), proximal sensors (EM38-sensor, NIR-sensor) and products of remote sensing (e.g., soil, phenology, yield maps). Because ECa is sensitive to numerous soil properties, such as texture (i.e., clay content), mineralogy, soil moisture and salinity (Corwin and Lesch 2005), its

use may be problematic in hilly to undulating young morainic soil landscapes composed of closely linked wet, boggy depressions and kettle holes with loamy, clayey peaks and plateaus, such as in north-eastern Germany (Lamp et al. 2004).

We present a model for functional soil mapping at the field-scale for precision farming based on multitemporal remote sensing data analysis and GIS spatial data modelling. The objectives are (i) to demonstrate the potential of multitemporal soil pattern analysis in comparison with monotemporal analysis, (ii) to generate functional soil maps based on identified soil reflectance patterns and related soil properties, and (iii) to improve these soil maps based on the detected static homogenous soil pattern. For data mining purposes, NDVI-thresholds and phenological data were used to select the most suitable RapidEye datasets out of 40. Because of the high spatial and temporal resolution of the multispectral imagery, the temporal-spatial static soil pattern could be derived using image-processing methods, such as standardized principal components analysis and per-Pixel-algorithms. This allowed the production of a highly significant functional soil map with respect to organic matter for the field outside of Borrentin in northeast Germany.

2 Materials & Methods

2.1 Study area

The multitemporal soil pattern approach was tested on a 131-ha agrarian field (53°48′9″N, 12°58′13″E) directly south of the village of Borrentin and 12 km south of Demmin in the north-eastern lowlands of Germany. The “Borrentin” field is located in the intensively used agricultural state Mecklenburg-Western Pomerania, consisting of 80.3% farmland, 19.5% grassland/pastureland and 0.2% other agrarian land use. In 2012, the main crops were cereal crops (55.5%), feed crops (19.3%), oleaginous fruits (18.6%), root crops (3.6%), legume crops (0.4%) and others (2.6%) (Statistisches Landesamt Mecklenburg-Vorpommern 2013).

Due to its geomorphological features, including (sandy-) loamy morainic parent material of the late Pleistocene, kettle holes and slightly undulated relief, the study site is characteristic of the young morainic soil-landscape of northern Germany (Bundesanstalt für Geowissenschaften und Rohstoffe 2006). Stagnosols, Luvisols and their transitional types evolved from unconsolidated glacial till and colluvial soils from eroded loamy material or deposits over former bogs (Zentrales Geologisches Institut 1942; Bundesanstalt für Geowissenschaften und Rohstoffe 2006). The elevation ranges between 39.3 m and 52.1 m above sea level (mean: 42.4 m; std. dev.: 2.4 m), and slope angle between 0° and 7° (mean: 1.1°, std. dev.: 1.1) (Bundesamt für Kartographie und Geodäsie 2014). At the field-scale, the “Borrentin” field has a low depression from southwest to northeast, with a high concentration of kettle holes and a more textured south-easterly adjacent area with relatively steep slopes and a few kettle holes concentrated in gullies (Figure 1) (Bundesamt für Kartographie und Geodäsie 2014).

Hydrologically, the Borrentin field drains subterraneously via a natural slope gradient from southwest to northeast, crossing the depression towards the creek “Galgenbach”, which flows into the River Peene 3 km northeast of the 32-km² Kummerower Lake (Bundesamt für Kartographie und Geodäsie 2012). The present climate is characterized by a long-term (1981-2010) mean temperature of 8.7° C and mean precipitation of 584 mm/yr, measured at the Teterow weather station, 26 km west of Borrentin (DWD 2014a, DWD 2014b).

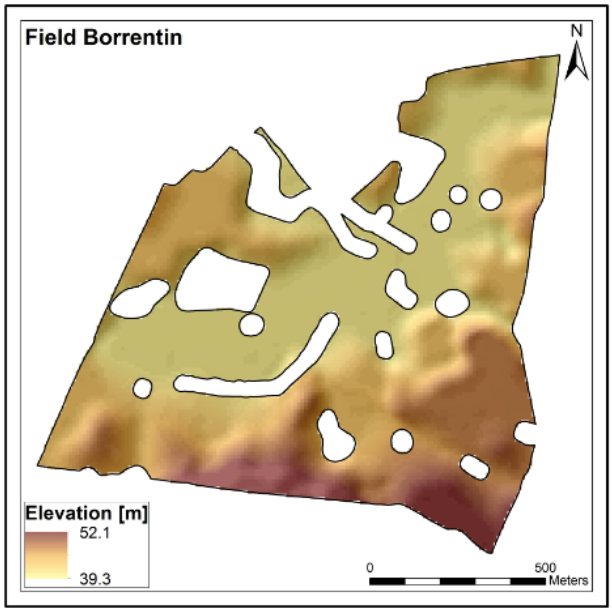

Figure 1: Digital Elevation Model (resolution: 10 m) of Field Borrentin (Bundesamt für Kartographie und Geodäsie 2014)

In general, the study area is located at the test site of DEMMIN® (Durable Environmental Multidisciplinary Monitoring Information Network; upper left corner: 54°2′N, 12°52′E, lower right corner: 53°45′N, 13°27′E), which was installed in 1999 by the German Aerospace Centre (DLR) as a calibration and validation test site for national and international remote sensing missions. Since the installation of the TERENO North-eastern German Lowland Observatory (TERENO-NE) in 2011, managed by the German Research Centre for Geosciences Potsdam (GFZ), both institutions have cooperated in the region of Demmin. The primary objective of TERENO is long term monitoring (>15 years) and analysis of environmental change. Further specific goals of the TERENO remote sensing research group at GFZ are (1) supplying environmental data for algorithm development in remote sensing and environmental modelling, with a focus on soil moisture and evapotranspiration, and (2) practical tests of remote sensing data integration in agricultural land management practices.

2.2 Baseline data

For model generation and validation as well as data interpretation, comprehensive soil sampling and analysis were conducted. Table 1 shows all input data and their specific characteristics.

Table 1: Baseline data and specific data characteristics

Category	Data	Characteristics

Remote Sensing	**RapidEye** Source: RapidEye Science Archive (RESA) & German Aerospace Centre (DLR)	• Spectral bands: 5 (B, G, R, RE, NIR) • 2009: 8 (April - September) • 2010: 6 (June - October) • 2011: 16 (March - November) • 2012: 10 (January - October)
Ground truth	**Phenological data** Source: German weather service (DWD) (DWD 2013)	• Observation stations: 5 (Dargun, Greifswald, Teusin, Tuetpatz, Tutow) • Initial date for each phenological macro stage per crop
	Crop data Source: Agrarservice Vorpommern GmbH	• Crop information (crop type)
	Meteorological data (precipitation) Source: German weather service (DWD) (DWD 2014a)	• Greifswald meteorological station
	Soil data Source: German Research Centre for Geosciences Potsdam (GFZ)	• Soil surface mixed sample: 170 • Soil properties: texture, soil acidity, organic matter content, and $CaCO_3$

2.2.1 Remote sensing data

To analyse the complexity of the soil and vegetation reflectance patterns, a multispectral, state-of-the-art sensor with high spatial and temporal resolution was needed. Due to its 5.5 days return frequency (at nadir), 6.5 m spatial resolution and the accessibility of the existing data archives, the RapidEye satellite system was chosen. In total, 43 radiometric calibrated and georeferenced RapidEye scenes (Level 1B, Level 3A) from April 2009 to October 2012 were obtained from the RapidEye Science Archive (RESA). After atmospheric correction using ATCOR for ERDAS IMAGINE and image to image co-registration using an in-house developed algorithm (Behling et al. 2014), coordinate transformation, cartographic projection and clipping to the extent of the study site, the resulting RapidEye subsets of the Borrentin field were used as the basis for further image analysis. From each RapidEye subset, NDVI-images were derived, and their descriptive statistics were analysed.

2.2.2 Vegetation data

Vegetation parameters, such as crop type, phenology and NDVI-index, characterize the vegetation and plant conditions at the time of acquisition. Based on the BBCH-scale (Meier 2001), for each phenological macro-stage ((0) germination, (1) leaf development, (2) tilling, (3) stem elongation, (4) booting, (5) inflorescence emergence/heading, (6) flowering/anthesis, (7) development of fruit, (8) ripening, and (9) senescence) of winter wheat and winter rape, the mean values of the initial dates were calculated from all phenological data from five observation stations (Table 1). These mean values represent the regional starting date of each phenological macro stage for each crop type. Therefore, all RapidEye subsets of the Borrentin field could be assigned to the corresponding BBCH-phenological stage based on the crop type. Finally, the annual crop information obtained was transformed into GIS-data through digitalization and vectorization.

2.2.3 Soil sampling and analysis

In October 2013 a total of 170 soil samples were collected from the study site. To receive a representative soil sample dataset a SW-NE-orientated grid sampling strategy was developed taking into account existing soil maps, digital elevation model and visible soil patterns based on soil colour.

Mean distance between neighbouring sampling locations was 66.3 m, ranging from 12.1 m to 98.4 m (std. dev. 12.36). The position of each sample was measured by GPS with an accuracy of approx. 5 m. To decrease the GPS-precision inaccuracy, a 5 m buffer around each soil sampling location was generated, expressing the location-specific mean values of digital data (e.g., multispectral bands, principal components) at sampling points. Later on these mean values were extracted for statistical analysis.

At each coordinate, five subsamples within a radius of 1 m and a depth from top to 10 cm were collected as one soil surface mixed sample, composed of 500 to 700 g of soil. Each sample represented approximately 0.78 ha. Following physical and chemical soil parameters were analysed by the soil-physical laboratory of the Institute of Ecology, Chair for Soil Conservation, University of Technology Berlin: (1) Particle size distribution using a combined sieve (fraction 0.063–2 mm) and pipette (fraction <0.063 mm) method (DIN ISO 11277), (2) soil acidity (pH) with 0.01 m CaCl2 (DIN ISO 10390; DIN EN 15933), (3) organic matter content (OM) by using the loss on ignition method (DIN 19684-3; DIN EN 15935; Ball 1964) and (4) carbon content ($CaCO_3$) (DIN EN ISO 10693). The results of particle size distribution were used for determination of soil texture classes according to the official German Soil Survey Description (AG Boden 2005).

2.3 Analysis workflow

In addition to data acquisition and preparation, the multitemporal approach presented here is composed of four analysing steps: (1) data mining, (2) image mining, (3) stability analysis, and (4) information extraction/statistical analysis/functional soil map generation.

2.3.1 Data mining / Selection of best suitable datasets

For multitemporal soil pattern analysis, the separation between the static soil pattern and the temporal pattern, which is derived from the (vital and senescent) vegetation, land management practices or clouds/cloud shadows, is the most important step. To facilitate the data mining process for the most suitable datasets, the time-series of 43 RapidEye subsets was filtered by (1) the threshold of the NDVI-MEAN (MEAN = arithmetic mean), (2) the threshold of the NDVI-SD (SD = standard deviation) and (3) the phenological situation per crop on the acquisition date. To be independent from field data the method is based only on image analysis and phenological data. An iterative visual analysis was performed, to define threshold values as basis for automated classification of (1) bare soil images and (2) images with vegetation/management effects.

First, the data with NDVI-MEAN values less than 0.2, indicating low vital vegetation, are selected for further analysis. Second, NDVI-SD (threshold = 0.07) allows the identification of disturbances from land management and atmospheric conditions (e.g., clouds or shadows). The wider the data dispersion from the average (arithmetic mean), the more probable is the inclusion of disturbing influences. The third selection criterion is the separation of bare soil images from ripe and senescent vegetation images. The time period from harvesting up to and including the phenological macro-stage

of germination assists with assigning low vegetation effects to vital, ripe and senescent plants. Furthermore, image enhancement methods, such as contrast stretching and false colour composite generation (Schowengerdt 2007), were used (1) to expose details of reflectance pattern and (2) to visually analyse management and vegetation effects (e.g., farming stripes or plant remains). Images with intolerable vegetation or management influences must be excluded.

For the Borrentin field, Figure 2 shows the NDVI-MEAN value (y_1-axis), the NDVI-SD value (y_2-axis), and the most suitable time-period based on the phenological and crop conditions (indicated by a blue box) for each RapidEye subset. Based on the NDVI-thresholds (MEAN 0.2, SD 0.07; indicated by an orange line) and on the phenological situation on the acquisition date (germination=0), the RapidEye subsets could be classified into two classes: (i) bare soil images (datasets below the orange line) and (ii) images with vegetation and/or management influences (datasets above the orange line). All subsets for which both NDVI-values are below the NDVI-threshold-line and which were taken in the most suitable time-period can be considered bare soil images with a tolerable vegetation effect, indicating that there was no significant vegetation influence disturbing the soil pattern detection.

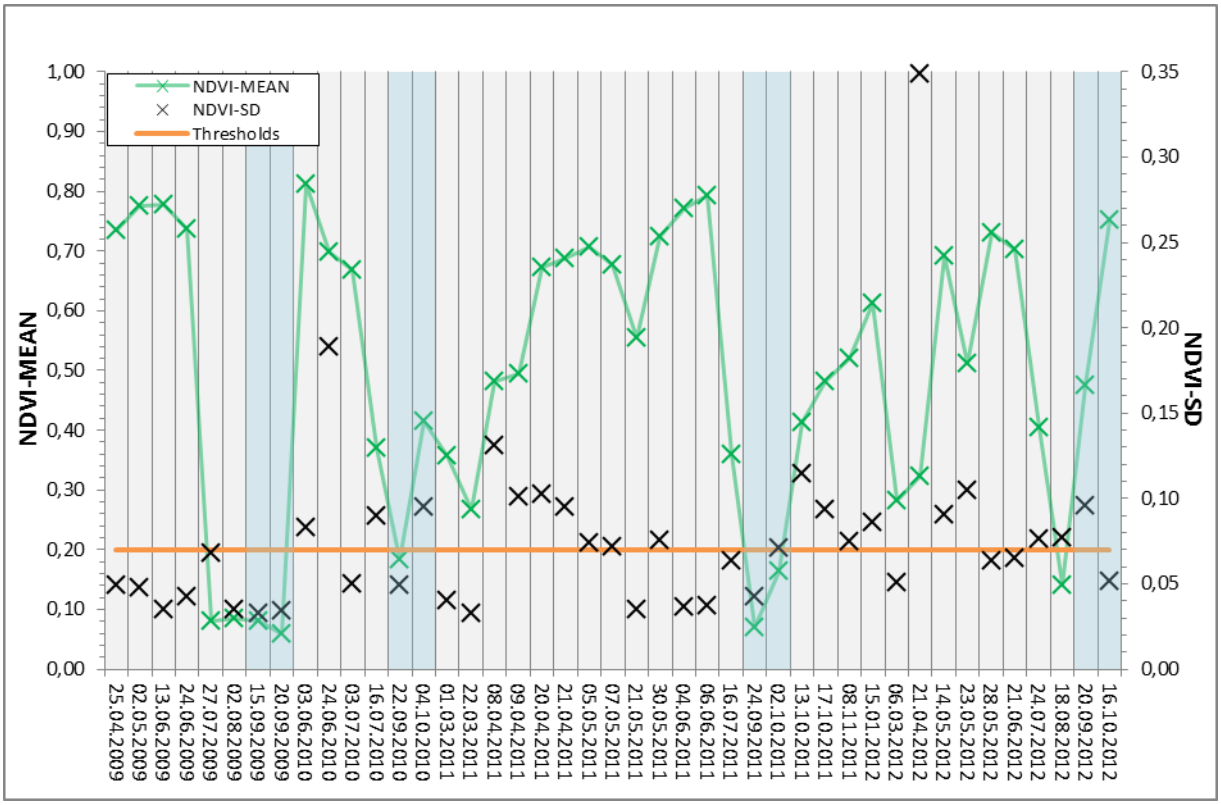

Figure 2: NDVI-threshold values and the most suitable time period (blue box) for each RapidEye-subset

Due to these three data selection criteria, the time series of RapidEye datasets could be split into 5 bare soil images (15/09/2009, 20/09/2009, 22/09/2010, 24/09/2011, and 02/10/2011), 1 bare soil image with strong management influence (18/08/2012), 29 vegetation images (25/04/2009, 02/05/2009, 13/06/2009, 24/06/2009, 02/08/2009, 03/06/2010, 03/07/2010, 16/07/2010, 04/10/2010, 01/03/2011, 22/03/2011, 09/04/2011, 20/04/2011, 21/04/2011, 05/05/2011, 07/05/2011, 21/05/2011, 04/06/2011, 06/06/2011, 13/10/2011, 17/10/2011, 08/11/2011, 15/01/2011, 06/03/2012, 14/05/2012,

28/05/2012, 21/06/2012, 24/07/2012, and 16/10/2012), and 8 cloudy scenes (27/07/2009, 24/06/2010, 08/04/2011, 30/05/2011, 16/07/2011, 21/04/2012, 23/05/2012, and 20/09/2012) were clearly identified. For each of those classes, Table 2 and Figure 3a, 3b, and 3c demonstrate exemplary RapidEye subsets and their filtering characteristics (NDVI-values and phenological macro-stage) as well as comments based on visual evaluation. The NDVI-SD of the image from 18/08/2012 (0.08) indicates too much variation for a bare soil image with a static pattern, which is supported by the previously mentioned image enhancement methods. The enhanced image showed detailed temporal patterns, such as farming stripes, which overlay the soil pattern in the eastern part of the field. Due to presented data selection method, the RapidEye subsets with a primarily temporal pattern, from vegetation, clouds, shadows or land management practices, could be identified and were excluded from further analysis because of their negative effects on the soil reflectance pattern detection.

Table 2: Example of NDVI-values and BBCH-phenological stages

BBCH-scale: (0) germination, (1) leaf development, (2) tilling, (3) stem elongation, (4) booting, (5) inflorescence emergence/heading, (6) flowering/anthesis, (7) development of fruit, (8) ripening and (9) senescence (Meier 2001)

RapidEye subsets of Borrentin					
acquisition date	**NDVI-MEAN**	**NDVI-SD**	**BBCH**	**class**	**visual evaluation**
15/09/2009	**0.08**	**0.03**	**0**	**bare soil image**	**bare soil**
20/09/2009	**0.06**	**0.03**	**0**	**bare soil image**	**bare soil**
22/09/2010	**0.18**	**0.05**	**0**	**bare soil image**	**bare soil**
01/03/2011	0.36	0.04	1-3	image with vegetation/management effects	vegetation 1-2
24/09/2011	**0.07**	**0.04**	**0**	**bare soil image**	**bare soil**
02/10/2011	**0.16**	**0.07**	**0**	**bare soil image**	**bare soil**
28/05/2012	0.73	0.06	5-7	image with vegetation/management effects	vegetation 3-8
21/06/2012	0.70	0.07	5-7	image with vegetation/management effects	vegetation 3-8
24/07/2012	0.40	0.08	8-9	image with vegetation/management effects	vegetation 9
18/08/2012	0.14	0.08	0	image with vegetation/management effects	bare soil management

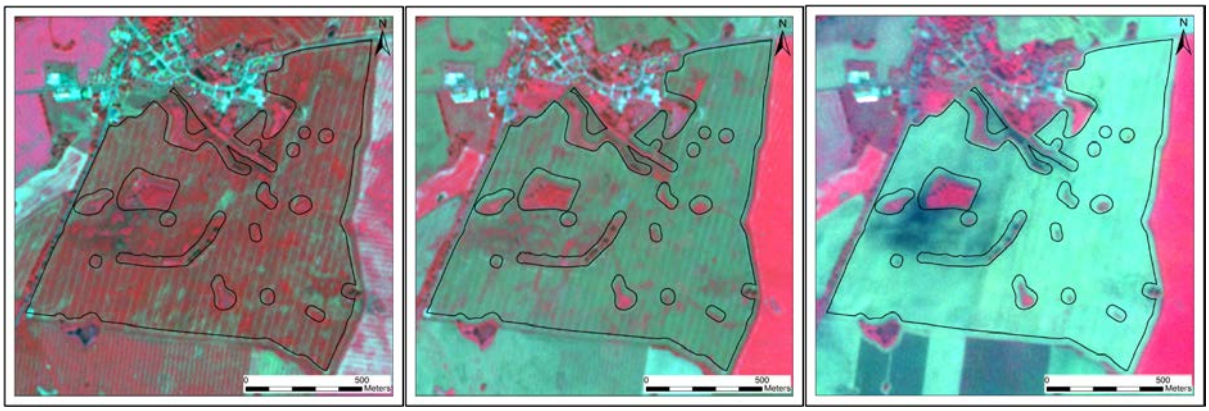

Figure 3a: Images with vegetation and/or land management influences (left to right: 21/06/2012, 24/07/2012, and 18/08/2012)

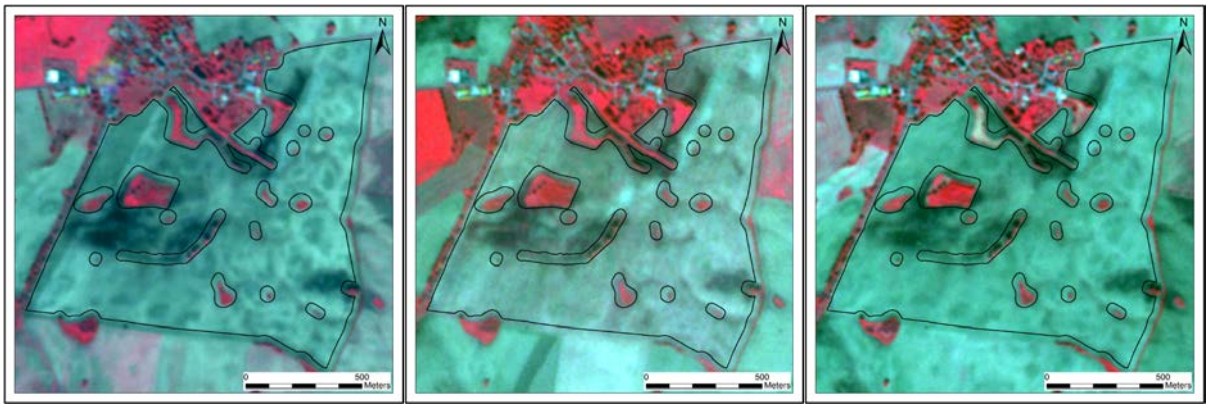

Figure 3b: Bare soil images (left to right: 15/09/2009, 22/09/2010, and 24/09/2011)

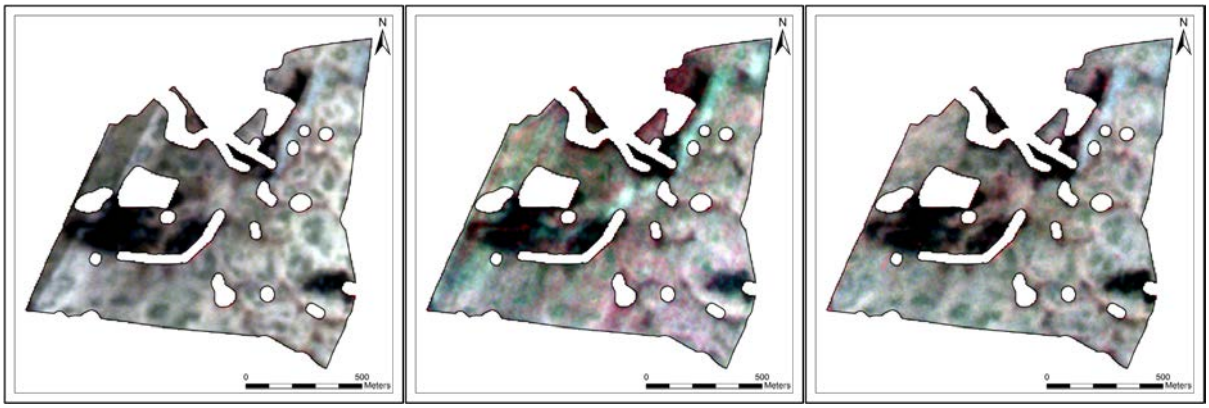

Figure 3c: Static and temporal patterns after image enhancement (left to right: 15/09/2009, 22/09/2010, and 24/09/2011)

In addition to vegetation and land management, variation in surface soil moisture also affects soil reflectance patterns, requiring an evaluation of the influence of soil moisture by comparing the preselected bare soil images with precipitation data because of the strong dependence between precipitation and surface soil moisture in relation to soil texture and relief position (Figure 1). The comparison of the amount of precipitation over the three days before image acquisition among all 5 selected bare soil subsets (Table 3) demonstrates that the precipitation amounts and consequently the soil moisture levels on 15/09/2009 (6.7 mm) and 22/09/2010 (6.1 mm) are quite similar in rainfall amount, distribution and intensity and that both are definitely more moist than the conditions on 24/09/2011 (0.3 mm), 20/09/2009 (0 mm) and 02/10/2009 (0 mm). For all 5 bare soil images, no rainfall occurred in the 24 hours before image acquisition.

Table 3: Amount of precipitation (mm) at the Greifswald meteorological station (DWD 2014a)

	Amount of precipitation [mm]					
Acquisition date	**Last 24 h**	**Last 2 days**	**Last 3 days**	**Last 6 days**	**Last 7 days**	**Last 14 days**
15/09/2009	0	5.6	6.7	6.7	6.7	29.5
20/09/2009	0	0	0	0	5.6	7.7
22/09/2010	0	4.7	6.1	6.1	8.7	35.9
24/09/2011	0	0.2	0.3	6.1	6.2	7.1
02/10/2011	0	0	0	0	0	6.1

For further spatial analysis of reflectance pattern and their relationships to soil properties, each identified bare soil image (best-suitable dataset) was used separately. Furthermore, a multitemporal

bare soil image, created by stacking all channels of each selected most suitable bare soil subset, is analysed. The resulting multitemporal-stacked image, consisting of 25 stacked bands, includes soil patterns with natural soil moisture fluctuations and essentially no management or vegetation influences.

2.3.2 Image mining / Detection of soil reflectance pattern

Principal components analysis (PCA) is one of the best methods to study correlated multidimensional data without harming all multispectral band information (Panda et al. 2010). “It is a way of identifying patterns in data, and expressing the data in such way as to highlight their similarities and differences” (Smith 2002). By removing redundant information from all spectral bands, the number of dimensions is reduced without significant loss of information. PCA is typically used to identify factors that describe spectral variance, to reveal the underlying dimensionality of multivariate data and to compress image data (Mulla 2013; Abdel-Kader 2011). Applying PCA on a simply stacked image consisting of multispectral data from multiple dates, a spectral-temporal transformation is performed. Because of the two coupled dimensions, interpretation might be difficult (Schowengerdt 2007). However, based on the assumption that the percentage area of change is relatively smaller than the percentage area of no change, stable areas will appear in the lower-order PCs, and changing areas in the higher-order PCs (Richards 1984; Ingebritsen and Lyon 1985). Due to the previously mentioned elimination of the negative influences from the soil pattern detection, this assumption is considered valid for the presented multitemporal approach. For more improvement in signal to noise ratio and image enhancement as well as for better results in the respective alignment along the object of interest, this procedure can be standardized by using the correlation matrix as an alternative to the common unstandardized method using the covariance matrix (Li and Yeh 1998; Singh and Harrison 1985; Fung and LeDrew 1987; Eastman and Fulk 1993). In this way, the original bands are effectively normalised to equal and unit variance, which might be an advantage when data with different dynamic ranges are combined (Schowengerdt 2007). Fung and LeDrew (1987) stated that the first four components can store greater than 95% of the total variance, and the remaining components contain very little valuable information for land change studies.

To detect the static soil pattern, the data dimensionality of the stacked image was reduced by performing standardised PCA. Based on the correlation matrix, twenty-five standardised principal components (PCsts 1-25) were calculated from the transformation of the 25 bands of the bare soil layer stack. The first five PCsts contain 99.64% of the total variance. Beginning with PCst 6, the data noise visibly increases (Figure 4); therefore, PCsts 1-5 were selected for subsequent statistical analysis. Figure 5 shows the three channel combinations of PCsts 1-5, which improve the visibility of the reflectance pattern.

For monotemporal analysis, standardised PCA was also applied for each bare soil image based on its own correlation matrix.

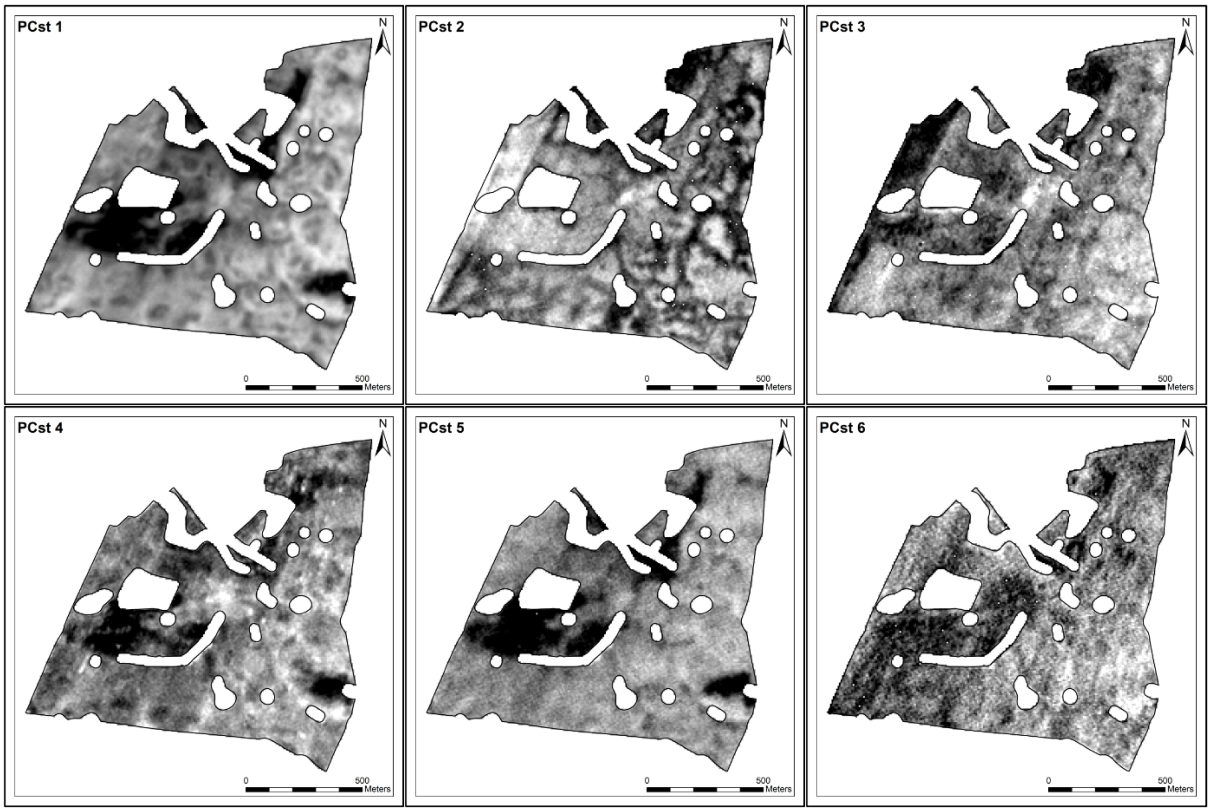

Figure 4: Image of PCsts 1-6

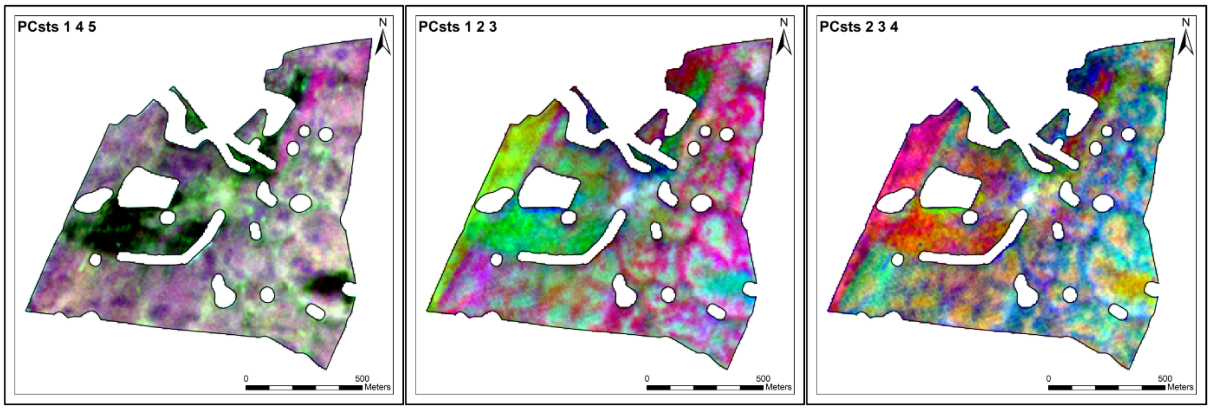

Figure 5: Image of the combined PCsts 1-5

2.3.3 Stability analysis / Temporal-spatial analysis of soil reflectance pattern

The multitemporal approach offers the possibility of evaluating the temporal-spatial stability of the soil reflectance pattern using change detection methods. For that reason, statistical per-pixel analysis was applied to preselected bare soil images. First, for each channel, one stacked image was created, consisting of the same channels of each bare soil subset. Second, for each stacked image, the standard deviation (SD) per pixel was calculated. Low standard deviation per pixel indicates high spatiotemporal stability. The lower the SD per pixel, the more static the reflectance pattern is. To combine the obtained pattern stability information, the resulting SD data of each channel were normalised by dividing by the corresponding SD maximum value. Thus, the SD data of each channel were scaled between 0 and 1, and disproportionate influence of channels with higher SD values due

to spectral characteristics was eliminated. Next, the arithmetic mean (MEAN) per pixel was calculated from all normalised SD per pixel images. The resulting image reflects the overall stability of the spatiotemporal pattern.

2.3.4 Information extraction / Statistical analysis / Functional soil map generation

For further statistical analysis, at every sampled soil point, the location-specific mean values of all standardised principal components of every monotemporal bare soil image and of the multitemporal bare soil stack images as well as all previously calculated absolute and normalized stability parameters (SD-per-channel, MEAN-of-all-SD-per-channel) were extracted. From 170 sampling sites, the descriptive statistics of each soil property variable were computed. Table 4 shows the mean, standard deviation, coefficient of variation, skewness, minimum and maximum of all soil parameters. Due to low occurrence of $CaCO_3$ data (12% of all soil samples) and due to low $CaCO_3$-content (Mean 3.3%, SD 2.4%), the topsoil layer of the Borrentin field could be assumed to be essentially free of $CaCO_3$.

Table 4: Descriptive statistics of soil parameters (SD: standard deviation; CV: coefficient of variation)

Soil parameter		Mean	SD	CV [%]	Skew	Min	Max
OM [%]	N = 170	5.38	7.66	58.72	4.70	1.52	54.82
pH	N = 170	6.52	0.50	0.25	-0.17	4.97	7.54
$CaCO_3$ [%]	N = 20	3.28	2.37	5.61	0.28	0.30	7.50
Clay [%]	N = 162	11.92	3.94	15.55	0.76	4.07	25.51
Silt [%]	N = 162	29.43	6.36	40.47	1.06	12.37	51.99
Sand [%]	N = 162	58.64	8.33	69.38	-1.06	24.81	82.52

Because soil parameters are typically not normally distributed, Spearman rank order correlation analysis was performed to examine the relationship between the soil parameters and the standardized principal components of the monotemporal and multitemporal images. The non-parametric Spearman´s rank correlation coefficient (r_s) characterizes here the strength of the observed relationships, at a 99% confidence level. The identified highly significant correlations ($r_s \leq -0.7$ or $r_s \geq 0.7$) were analysed in more detail using simple linear and non-linear regressions. The coefficient of determination (R^2) was used to evaluate prediction quality. The model with the highest R^2-value was chosen as the best prediction model. The efficiency of the prediction method (here, the obtained regression equation) was statistically evaluated by using leave-one-out cross-validation (Isaaks and Srivastava 1989). Therefore, the root mean square error (RMSE) was calculated. The lower the RMSE value, the more robust the prediction model is.

The resulting regression equations of those soil variables that showed higher significant correlations with the best predicting standardized principal components were applied to the corresponding monotemporal and multitemporal images to generate functional soil maps.

To eliminate any still existing temporal influence and to improve the prediction model, the normalized stability parameter MEAN-of-all-SD-per-channel was used to identify the threshold separating static and temporal reflectance patterns. For this purpose, the MEAN-of-all-SD-per-channel dataset was divided by percentiles (100-quantiles) into 100 groups of equal frequency 1%-segments. The

percentile value represents the separating-thresholds, below which all data are considered static and above which all data are considered temporal. Each extracted percentile value was applied to the input data by eliminating all sampling point data above the threshold and then was subsequently tested in the previously described regression prediction model with the same quality assessment and functional soil mapping procedure.

3 Results and Discussion

For soil parameter prediction modelling based on mono- and multitemporal bare soil images, it is necessary to identify those soil parameters that explain soil reflectance patterns. The obtained best model allows functional soil mapping at high accuracy. Analysing the temporal-stability of soil reflectance patterns and excluding detected temporal effects from the prediction model could improve the functional soil map.

3.1 Relationships between soil properties and multitemporal/monotemporal bare soil images

To understand the origin of the PCA-detected soil reflectance pattern, the relationships between the values of the standardised principal components and the laboratory-analysed soil parameters were statistically evaluated. Table 5 summarizes the relationships between soil properties and the standardised PCs of multitemporal and monotemporal bare soil images using the non-parametric Spearman´s rank correlation coefficient.

Table 5: Spearman-Rho correlation between soil parameters and standardized PCs of multitemporal and monotemporal bare soil images

(* significant at probability level 0.05, ** significant at probability level 0.01)

Bands	OM [%]	pH	$CaCO_3$ [%]	Clay [%]	Silt [%]	Sand [%]
Multitemporal						
PCst 1	**-0.797****	-0.162*	**0.539****	-0.378**	-0.155*	0.299**
PCst 2	0.200**	0.11	0.045	0.337**	-0.089	-0.097
PCst 3	-0.533**	-0.01	0.254	-0.092	**-0.238****	0.209**
PCst 4	-0.577**	**-0.205****	0.263	**-0.453****	-0.190*	**0.383****
PCst 5	-0.762**	-0.12	0.448*	-0.265**	-0.123	0.212**
15/09/2009						
PCst 1	-0.773**	-0.171*	**0.498***	-0.417**	-0.132	0.307**
PCst 2	**-0.781****	-0.107	0.394	-0.316**	-0.118	0.243**
PCst 3	-0.503**	**-0.241****	0.130	**-0.473****	-0.113	**0.335****
PCst 4	-0.447**	-0.201**	0.022	-0.428**	**-0.161***	0.332**
PCst 5	0.692**	0.150	-0.348	0.277**	0.129	-0.217**
20/09/2009						
PCst 1	**-0.756****	-0.169*	**0.543***	**-0.361****	-0.116	0.266**
PCst 2	-0.745**	-0.162*	0.471*	-0.259**	-0.102	0.194*
PCst 3	0.428**	**0.230****	-0.148	0.334**	**0.163***	**-0.290****
PCst 4	-0.495**	-0.215**	0.254	-0.329**	-0.097	0.241**
PCst 5	0.697**	0.175*	-0.436	0.238**	0.042	-0.155*

22/09/2010						
PCst 1	**-0.763****	-0.147	**0.536***	-0.286**	-0.247**	0.320**
PCst 2	-0.605**	-0.094	0.396	-0.125	-0.225**	0.203**
PCst 3	-0.015	**0.302****	0.442	**0.288****	-0.006	-0.158*
PCst 4	-0.516**	-0.104	0.463*	-0.172*	-0.180*	0.201*
PCst 5	-0.593**	-0.269**	0.373	-0.270**	**-0.256****	**0.329****
24/09/2011						
PCst 1	**-0.777****	**-0.197****	**0.632****	**-0.416****	-0.127	**0.302****
PCst 2	-0.704**	-0.165*	0.466*	-0.327**	-0.139	0.261**
PCst 3	0.007	-0.168*	-0.141	-0.386**	-0.036	0.241**
PCst 4	-0.245**	-0.176*	-0.086	-0.224**	-0.129	0.246**
PCst 5	0.628**	0.124	-0.209	0.266**	**0.180***	-0.260**
02/10/2011						
PCst 1	**-0.768****	-0.152*	**0.619****	-0.368**	-0.122	0.272**
PCst 2	-0.352**	-0.167*	0.115	**-0.522****	-0.087	0.361**
PCst 3	-0.699**	0.034	0.493*	0.031	-0.080	0.022
PCst 4	0.348**	**0.274****	-0.211	0.502**	0.117	**-0.369****
PCst 5	-0.634**	-0.135	0.379	-0.174*	**-0.131**	0.177*

For the multitemporal stacked image, this coefficient revealed that OM, pH, $CaCO_3$, clay, silt and sand were most strongly significantly correlated with the following spectral data: PCst 1 (OM), PCst 4 (pH), PCst 1 ($CaCO_3$), PCst 4 (clay), PCst 3 (silt) and PCst 4 (sand). Strong correlations ($r_s \leq -0.7$ or $r_s \geq 0.7$) were seen between OM and PCst 1/PCst 5 (r_s = -0.797/-0.762). Other soil parameters showed moderate correlations (r_s = ~±0.5), for instance, $CaCO_3$ with PC 1 (r_s = 0.539) and clay with PCst 4 (r_s = 0.453), and weak correlations (r_s = ±0.3 - ±0.4) were seen for sand (r_s = 0.383). Silt (r_s = -0.238 with PC 3) and pH (r_s = -0.205 with PC 4) were the soil properties with the lowest significant correlation coefficient. Negative correlations indicated that small values of the standardised PCs corresponded to high values of soil properties. The darker the reflectance pattern, the higher the soil parameter value is.

Similar to the multitemporal image, in all monotemporal images, strong correlations were observed only for OM (PCst 1, PCst 2, PCst 3, and PCst 5). OM generally had the highest correlation with PCst1 (r_s = -0.756 - -0.777), with the exception of one date, when it was more strongly correlated with PCst 2 (r_s = -0.781; 15/09/2009). As before, moderate correlations were found for $CaCO_3$ with PCst 1 (r_s = 0.498 - 0.632) and clay with PCsts 1-3 (r_s = -0.361 - -0.522). Weak correlations were observed for sand (r_s = 0.302 – 0.335; r_s = -0.369) and for pH on one date (r_s = 0.302; 22/09/2010). A very low significant relationship was detected for silt (r_s = -0.131 - -0.256; r_s = 0.163 - 0.256).

Due to the results of the non-parametric Spearman´s rank correlation coefficient calculations, the soil parameters and standardised PCs with significant high correlations were considered highly valuable for deeper statistical analysis and prediction model generation. OM and PCst 1/PCst 5 were used for the multitemporal analysis, and for the monotemporal images, OM and PCst 1 (15/09/2009, 20/09/2009, 22/09/2010, 24/09/2011, and 02/10/2011), PCst 2 (15/09/2009, 20/09/2009, and 24/09/2011) and PCst 3 (02/10/2011) were used. The low to moderate correlations indicate that certain soil parameters (pH, $CaCO_3$, clay, silt, and sand) are not suitable for functional soil mapping in this study, possibly because of the generally limited spectral resolution of the broadband multispectral sensor. Using hyperspectral sensors might be more promising for these soil parameters.

Visualising the scatterplots of each soil variable with each PCst reveals that, in total, no linear relationship between the soil parameters and the standardised PCs could be recognised. Further, no strong evidence of non-linear relationships between the already excluded soil properties (pH, $CaCO_3$, clay, silt, and sand) and the standardised PCs could be identified. In comparison, the scatterplots of OM and the previously selected standardised PCs revealed non-linear relationships, expressed by power functions. To simplify further statistical analysis, the simple non-linear regression models were log10-transformed to simple linear regression models. To detect the best prediction model for OM, Table 6 compares the R^2 and RMSE values of the transformed linear regression models between the multi- and monotemporal images.

Table 6: R^2 and RMSE for the relationship between OM (dependent variable) and the standardized PCs of the multitemporal and monotemporal images (independent variable)

Multitemporal			**15/09/2009**			**20/09/2009**			**22/09/2010**			**24/09/2011**			**02/10/2011**		
Bands	**R^2**	**RMSE [%]**	**Bands**	**R^2**	**RMSE [%]**	**Bands**	**R^2**	**RMSE [%]**	**Bands**	**R^2**	**RMSE [%]**	**Bands**	**R^2**	**RMSE [%]**	**Bands**	**R^2**	**RMSE [%]**
PCst 1	**0.795**	**7.59**	**PCst 1**	0.762	8.17	**PCst 1**	0.773	7.98	**PCst 1**	0.735	8.63	**PCst 1**	0.787	7.73	**PCst 1**	0.746	8.44
PCst 5	0.763	7.94	**PCst 2**	0.766	8.10	**PCst 2**	0.755	8.29	**PCst 2**	0.651	9.90	**PCst 2**	0.759	8.23	**PCst 3**	0.673	9.57

Thus, for all OM-samples, significant (p-value <2.2e-16) and robust linear regression models with a coefficient of determination $R^2 \geq 0.673$ and RMSE ≤ 9.90% were calculated. According to the highest coefficient of determination ($R^2 = 0.795$), the multitemporal-stacked image with the first standardised PC is the better option for functional soil mapping compared with monotemporal images ($0.735 \leq R^2 \leq 0.787$). In addition, the prediction model based on the multitemporal-stacked image is the most robust (RMSE = 7.59%).

Similar non-linear relationships were observed by Spielvogel et al. (2004) for the relation between OC content and soil lightness and by Konen et al. (2003) for OC content and Munsell value, chroma, and reflectance of agrarian soils in Iowa. Hummel et al. (2001) applied logarithmic-transformation to a non-linear relationship between soil organic matter and NIR-data.

An increase in OM content is correlated with a decrease in the spectral reflectance value of PCst 1, and consequently, the darker the soil pattern, the higher the OM content, and the lighter the soil pattern, the lower the OM content.

Although the calculated regressions are significant, with a high coefficient of determination, some samples with log OM contents between 0.3% and 0.7% have differences in their log PCst 1-spectral reflectance values. This high variance indicates that the PCst 1 spectral reflectance is influenced by several other parameters. Although the correlations between the texture parameters (clay, silt, and sand) and PCst 1 were not significant ($R^2 \leq 0.185$), the spectral reflectance (soil lightness) affecting the parameters could be $CaCO_3$ and texture, where the OM content is the main determining variable, followed by $CaCO_3$, clay and the low but significant influence of silt and sand contents (Spielvogel et al. 2004). The darkening effect of Fe-oxides on soil brightness (e.g., hematite) (Schwertmann 1993) does not occur here, due to the glaciomorphological and pedological genesis of the young morainic soil landscape of northern Germany.

To generate SSM user-friendly functional soil maps based on real OM values, it was necessary to re-transform the obtained linear regression function and the coefficients back to a non-linear regression function. Based on the extracted and re-transformed prediction function of the multitemporal-stacked image, a functional soil map for OM was produced and classified with adaption to the official German Soil Survey Description (AG Boden 2005) (Figure 6).

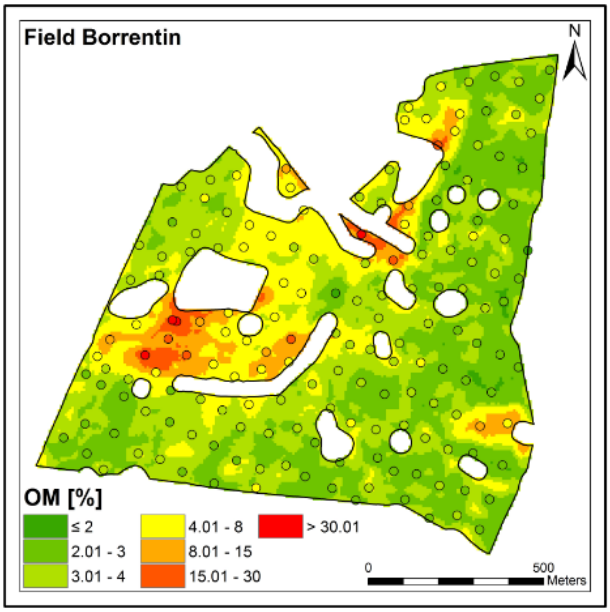

Figure 6: Functional soil map regarding OM based on the predicting regression equation of the multitemporal image and PCst 1 (OM classification adapted to the official German Soil Survey Description with soil sampling results)

Comparing the classified soil map with the laboratory measured OM-values shows that they are in accordance, particularly in the western portion of Borrentin field. There are still some prediction errors in the eastern portion, most likely caused by temporal effects. To understand this prediction uncertainty, a deeper analysis of the temporal-spatial stability of the reflectance patterns is necessary.

3.2 Stability analysis

To evaluate the temporal-spatial stability of the soil reflectance patterns, statistical pixel-wise analyses were applied on the multitemporal bare soil image. Further, the possibility of prediction model improvement was tested by stepwise eliminating the identified temporal effects.

Figure 7 reveals that the visible spectrum (B, G, and R) shows a similar distribution of the spatiotemporally static reflectance patterns of bare soils. In comparison, the images of the RE- and NIR-channels exhibit either similar or different stability. The overall stability, which reflects the average spatiotemporal stability of the bare soil reflectance pattern, was calculated as a mean of all SD-images (B, G, R, RE, NIR) (Figure 7).

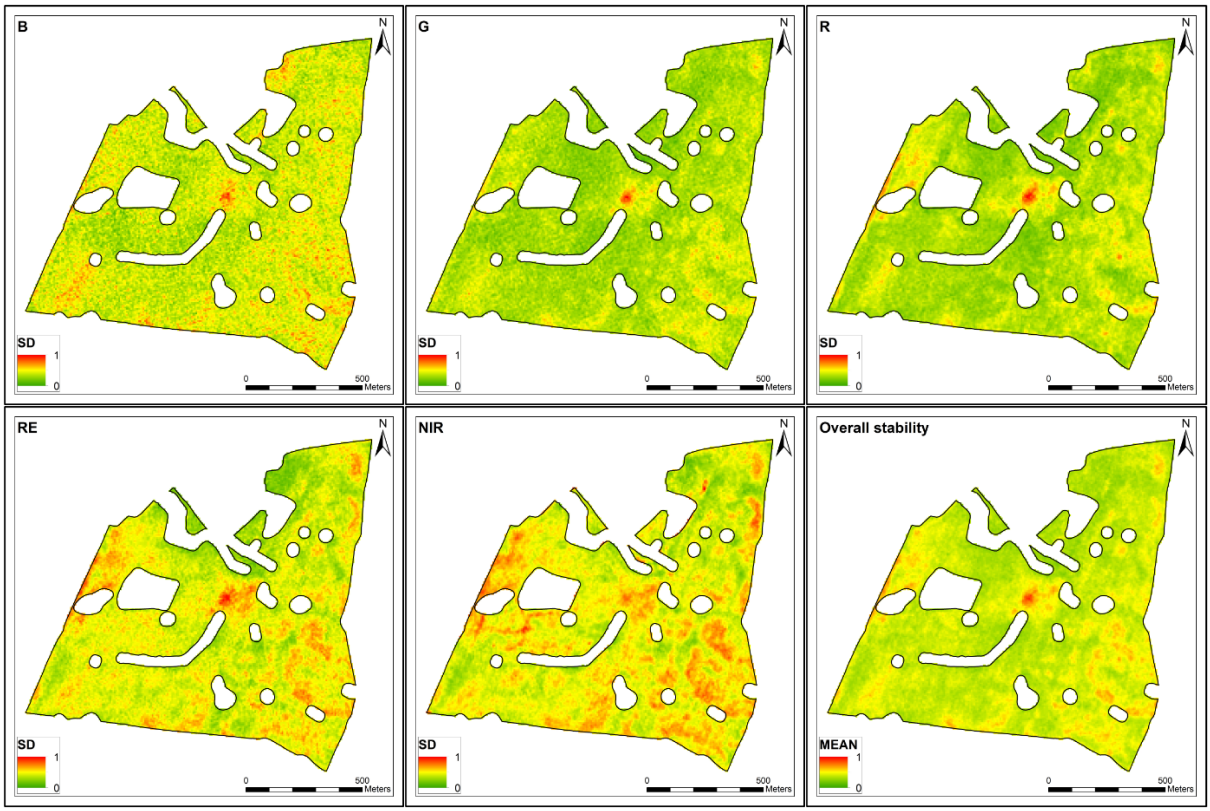

Figure 7: Spatiotemporal stability of the bare soil reflectance pattern, divided by channel (green: low SD, red: high SD; data are normalized) and spatiotemporal overall stability of the bare soil reflectance pattern as a mean of all SD-images (green: low mean value, red: high mean value; data are normalized)

We assume that the pattern with a high SD results from temporal effects, originating in the cause and effect relationships of relief, soil moisture, soil texture and vegetation (e.g., upcoming plants). In addition, land management (e.g., fertilisation and soil cultivation) are also causing the temporal pattern.

Because of the previous assumption it is necessary to improve the developed prediction model for OM by excluding the strong temporal effects, which is allowed due to multitemporal data. Based on the spatiotemporal overall stability image (Figure 7), percentile-thresholds were statistically (stepwise per percentile) tested to separate static (low SD mean value) from temporal patterns (high SD mean value) (Figure 8). Applying the 67%-threshold, the OM prediction model was improved by approximately 2% (R^2 = 0.795 to R^2 = 0.814) with a weak loss of model robustness of approximately 1.5% (RMSE = 7.59% to RMSE = 9.04%). This relatively low model improvement is due to previous filtering of the input datasets to detect the bare soil images with very low temporal effects.

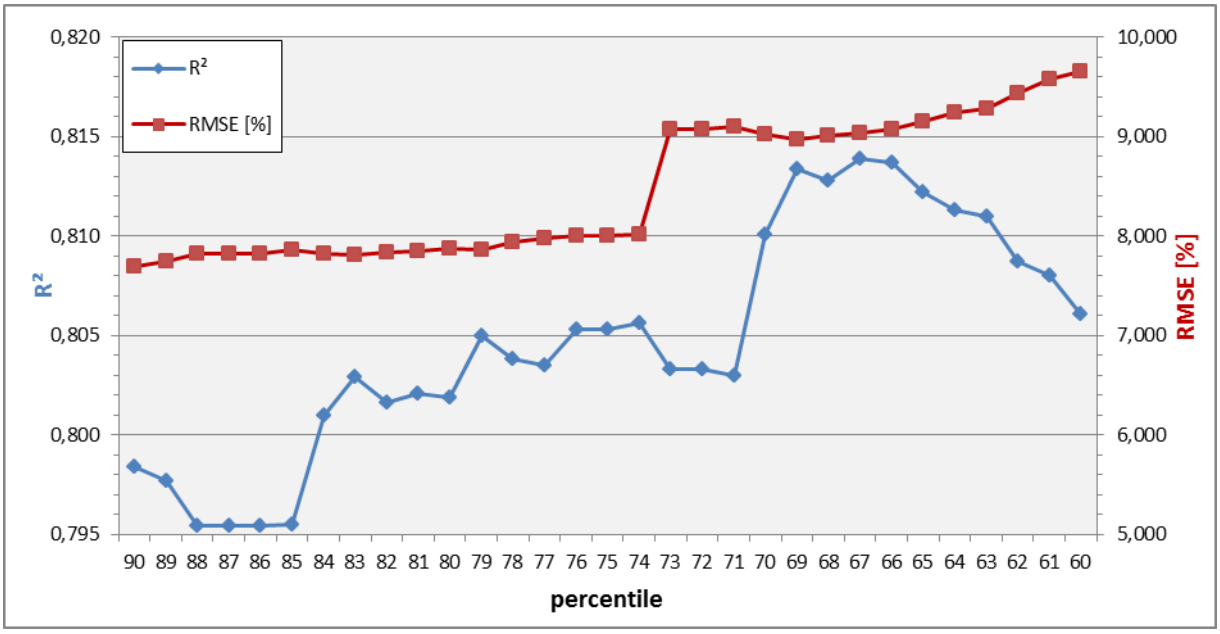

Figure 8: Examples of the splitting thresholds (percentiles 90 to 60) and their corresponding R^2 and RMSE values

To achieve the greatest model improvement based on the 67%-threshold of the spatiotemporal overall stability image, the soil sampling points (as model input data) within the identified temporal pattern were excluded from the further modelling steps. These excluded points are located in the total range of OM-values. In this case, the soil sample quantity was reduced from 170 to 122 samples (Figure 9).

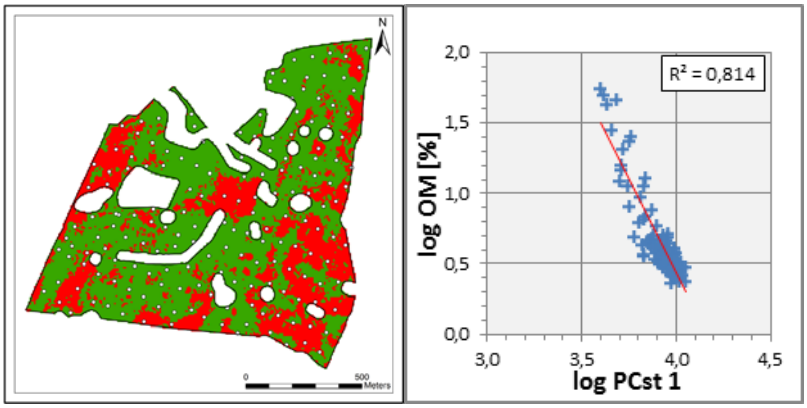

Figure 9: (left) Soil samples within the static and temporal reflectance pattern based on the 67%-threshold (green: static pattern; red: temporal pattern); (right) Scatterplot of the relationships between OM and standardized PC 1 of the multitemporal bare soil images based on the static soil pattern (threshold: 67%)

Figure 9 also demonstrates the improved prediction model for OM and PCst 1 of the multitemporal dataset based on the 67%-threshold. A functional soil map of OM was derived from the enhanced regression equation and was also classified with adaption to the official German Soil Survey Description (AG Boden 2005) (Figure 10). Especially in the eastern, more textured portion of Borrentin field, the resulting functional soil map (based on the 67%-threshold) was improved for low OM-values compared with the previous map (Figure 6).

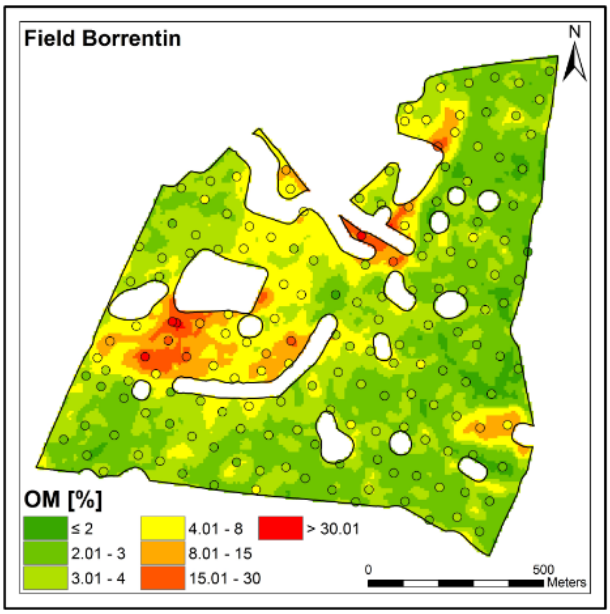

Figure 10: Functional soil map for OM based on the predicting regression equation of the multitemporal image and PCst 1 (threshold: 67%) (OM classification adapted to the official German Soil Survey Description with soil sampling results)

4 Conclusions & Outlook

This study has provided support for the concept that multitemporal analysis of multispectral remote sensing data, such as RapidEye imagery, is more suitable than monotemporal analysis for the extraction of spatially precise static soil patterns for functional soil mapping at the field-scale. Data pre-selection from the time-series using NDVI-thresholds and phenological macro-stages per crop on the acquisition date is essential to separate static from temporal reflectance patterns. Due to these selection methods, the bare soil images were accurately identified, and consequently, subsequent visual evaluation is no longer necessary. Statistical analysis demonstrated the existence of a non-linear relationship between OM and the standardised principal components with the best prediction results combined with PCst 1. The further analysed soil parameters (pH and texture) did not correlate sufficiently with the standardised principal components due to the spectral sensor resolution. $CaCO_3$ was at least moderately significantly correlated with the PCsts, but its presence was very limited (20 samples) in Borrentin field.

Based on the spectral reflectance pattern (static soil pattern) of PCst 1 and the OM soil sampling data, a functional soil map of OM distribution could be produced. This functional soil mapping could be improved by eliminating reflectance patterns with strong spatiotemporal variability using stepwise testing percentile-thresholds. For Borrentin field, 67%-threshold was determined to be the best threshold. The correlation in this study between the spectral data (spectral variance) of the first standardised principal component of the multitemporal bare soil layer stack and the soil surface organic matter might be applied to other agrarian fields in the young morainic soil-landscape of north-eastern Germany. For methods transfer at the field-scale as well as the landscape-scale, further investigations are necessary. Another advantage of standardised PCA is the possibility of transferring

the transformation parameters (correlation matrix) from one study area to another, thus securing methods transferability. Therefore, more soil sampling has been performed in 13 fields in the Demmin region. In addition, further analysis regarding the relationships between the static soil pattern and vegetation patterns should be performed, to gain knowledge concerning the transferability of soil surface patterns to deeper soil horizons because vegetation patterns might reflect the soil conditions of the deeper horizons (e.g., root zone), which could be recognized in the soil surface pattern. Furthermore, the analysis of soil reflectance pattern combined with DEM derived parameters could help to achieve a deeper understanding of the origin of soil reflectance pattern and their stability characteristics.

In the future, the resulting static soil (brightness) patterns and their derived high resolution functional OM soil maps could be used as ancillary data either in delineating management zones for site-specific management in precision agriculture (e.g., respective sowing intensity and fertilization distribution) or as an information input to prediction models (e.g., scorpan) as well as for soil survey preparation and the calculation of soil fertility. Mulla (2013) stated the importance of combining archived and historical remote sensing data with real-time and auxiliary data (e.g., crop yield maps, digital elevation models, soil series maps). Therefore, the static soil pattern might be highly valuable for improving decision-making in agricultural management.

Acknowledgements

We are grateful to have the chance to complete our research activities in the project area of the Terrestrial Environmental Observatory Northeast (TERENO NE). Further, we thank the German Aerospace Centre (DLR) for providing the data from the RapidEye Science Archive (RESA 617 FKZ) and also appreciate the cooperation of the agricultural company of Agrarservice Vorpommern GmbH. The comments of the editor and the referees are highly appreciated.

References

Abdel-Kader, F.H. (2011). Digital soil mapping at pilot sites in the northwest coast of Egypt: A multinomial logistic regression approach. *The Egyptian Journal of Remote Sensing and Space Science*, *14*(1), 29–40. doi:10.1016/j.ejrs.2011.04.001.

AG Boden (2005). Bodenkundliche Kartieranleitung. 5th ed., Schweizerbart´sche Verlagsbuchhandlung, Hannover. p. 438.

Ball, D.F. (1964). Loss-on-ignition as an estimate of organic matter and organic carbon in non-calcareous soils. *Canadian Journal of Soil Science, 15*, 84–92.

Behling, R., Roessner, S., Segl, K., Kleinschmit, B., Kaufmann, H. (2014). Robust automated image co-registration of optical multi-sensor time series data: Database generation for multi-temporal landslide detection. *Remote Sensing, 6* (3), 2572-2600. doi: http://doi.org/10.3390/rs6032572.

Birrell, S.J., Sudduth, K.A., Borgelt, S.C. (1996). Comparison of sensors and techniques for crop yield mapping. *Computers and Electronics in Agriculture, 14*(2-3), 215–233.

Bundesanstalt für Geowissenschaften und Rohstoffe (Eds.) (2006). Bodenübersichtskarte 1:200.000 (BÜK200) - CC2342 Stralsund. Hannover.

Bundesamt für Kartographie und Geodäsie (Eds.) (2012). Digitales Basis-Lanschaftsmodell (AAA-Modellierung - Basis-DLM (AAA)) - Mecklenburg-Vorpommern. Frankfurt am Main.

Bundesamt für Kartographie und Geodäsie (Eds.) (2014). DGM 10 - Vektordaten - Digitales Geländemodell Gitterweite 10m – Bundesrepublik Deutschland. Frankfurt am Main.

Corwin, D.L., Lesch, S.M., (2005). Apparent soil electrical conductivity measurements in agriculture. *Computers and Electronics in Agriculture, 46*, 11–43.

DIN 19684-3:2000-08. Methods of soil investigations for agricultural water engineering - Chemical laboratory tests – Part 3: Determination of the loss on ignition and the residue of soil after ignition.

DIN EN 15933:2012-11. Sludge, treated biowaste and soil - Determination of pH. German version EN 15933:2012.

DIN EN 15935:2012-11. Sludge, treated biowaste, soil and waste - Determination of loss on ignition. German version EN 15935:2012.

DIN EN ISO 10693:2014-06. Soil quality - Determination of carbonate content - Volumetric method (ISO 10693:1995). German version EN ISO 10693:2014.

DIN ISO 10390:2005-12. Soil quality - Determination of pH (ISO 10390:2005).

DIN ISO 11277:2002-08. Soil quality - Determination of particle size distribution in mineral soil material - Method by sieving and sedimentation (ISO 11277:1998 + ISO 11277:1998 Corrigendum 1:2002).

DWD (2013). Download of phenological data (2000-2012). Publication date: 13/03/2013. Last access: 18/07/2013.

DWD (2014a). Download of precipitation long-term mean values (1981-2010). Publication date: 19/11/2013. Last access: 29/01/2014.

DWD (2014b). Download of temperature long-term mean values (1981-2010). Publication date: 19/11/2013. Last access: 29/01/2014.

Eastman, J.R., Fulk, M. (1993). Long sequence time series evaluation using standardized principle components. *Photogrammetric Engineering and Remote Sensing, 59*, 991-996.

Franzen, D.W., Hopkins, D.H., Sweeney, M.D., Ulmer, M.K., Harvorson, A.D. (2002). Evaluation of soil survey scale for zone development of site-specific nitrogen management. *Agronomy Journal, 94*, 381–389.

Fung, T., LeDrew, E. (1987). Application of principal components analysis change detection. *Photogrammetric Engineering and Remote Sensing, 53*, 1649-1658.

Ge, Y., Thomasson, J.A., Sui, R. (2011). Remote sensing of soil properties in precision agriculture: A review. *Frontiers of Earth Science, 5*(3), 229-238. doi: 10.1007/s11707-011-0175-0.

Gotway, C.A., Ferguson, R.B., Hergert, G.W., Peterson, T.A. (1996). Comparison of kriging and inverse-distance methods for mapping soil parameters. *Soil Science Society of America Journal, 60*, 1237-1247.

Guo, Y., Shi, Z., Li, H.Y., Triantafilis J. (2013). Application of digital soil mapping methods for identifying salinity management classes based on a study on coastal central China. *Soil Use and Management, 29*, 445–456. doi: 10.1111/sum.12059.

Hummel, J.W., Sudduth, K.A., Hollinger, S.E. (2001). Soil moisture and organic matter prediction of surface and subsurface soils using an NIR soil sensor. *Computers and Electronics in Agriculture, 32*(2), 149–165. doi: 10.1016/S0168-1699(01)00163-6.

Ingebritsen, S.E., Lyon, R.J.P. (1985). Principal components analysis of multitemporal image pairs. *International Journal of Remote Sensing, 6*(5), 687-696. http://dx.doi.org/10.1080/01431168508948491.

Isaaks, E.H., Srivastava, R.M. (1989). An introduction to applied geostatistics. Oxford University Press, Oxford, UK. p. 561.

Konen, M., Burras, C., Sandor, J. (2003). Organic carbon, texture, and quantitative color measurement relationships for cultivated soils in north central Iowa. *Soil Science Society of America Journal, 67*, 1823–1830.

Lamp, J., Herbst, R., Reimer, G. (2001). Preciser and efficient soil surveys as basis for application maps in Precision Agriculture. In: Grenier, G., Blackmore, S. (Eds.). Proceedings of the 3rd European Conference on Precision Agriculture. Montpellier, 49-54.

Lamp, J., Herbst, R., Reimer, G. (2002). Digitale Hofbodenkarten. In: Werner, A., Jarfe A. (Eds.). Precision Agriculture. Herausforderung an integrative Forschung, Entwicklung und Anwendung in der Praxis – Tagungsband. *KTBL Sonderveröffentlichung, 038*, Bonn, Germany, 35-52.

Lamp, J., Herbst, R., Reimer, G. (2004). Digitale Hof-Bodenkarte. In: ZALF (Eds.). Managementsystem für den ortsspezifischen Pflanzenbau. Verbundprojekt pre agro. Abschlussbericht. 3-73.

Li, X., Yeh, A.G.O. (1998). Principal component analysis of stacked multi-temporal images for the monitoring of rapid urban expansion in the Pearl River Delta. *International Journal of Remote Sensing, 19*(8), 1501-1518. http://dx.doi.org/10.1080/014311698215315.

Lin, H.S., Bouma, J., Wilding, L., Richardson, J., Kutilek, M., Nielsen, D. (2005a). Advances in hydropedology. *Advances in Agronomy, 85*, 1–89.

Lin, H.S., Wheeler, D., Bell, J., Wilding, L. (2005b). Assessment of soil spatial variability at multiple scales. *Ecological Monographs, 182*, 271–290.

Liu, J., Pattey, E., Nolin, M.C., Miller, J.R., Ka, O. (2008). Mapping within-field soil drainage using remote sensing, DEM and apparent soil electrical conductivity. *Geoderma, 143*, 261–272.

López-Granados, F., Jurado-Expósito, M., Peña-Barragán, J.M., García-Torres, L. (2005). Using geostatistical and remote sensing approaches for mapping soil properties. *European Journal of Agronomy*, *23*(3), 279–289. doi:10.1016/j.eja.2004.12.003.

McBratney, A.B., Odeh, I.O.A., Bishop, T.F.A., Dunbar, M.S., Shatar, T.M., (2000). An overview of pedometric techniques for use in soil survey. *Geoderma, 97*, 293–327.

McBratney, A.B., Mendonça Santos, M.L., Minasny, B. (2003). On digital soil mapping. *Geoderma, 117*, 3–52. doi:10.1016/S0016-7061(03)00223-4.

Meier, U. (Eds.) (2001). Entwicklungsstadien mono- und dikotyler Pflanzen. BBCH Monografie. 2nd ed., Braunschweig. p. 165.

Mulder, V.L., de Bruin, S., Schaepman, M.E., Mayr, T.R. (2011). The use of remote sensing in soil and terrain mapping — A review. *Geoderma*, *162*(1-2), 1–19. doi:10.1016/j.geoderma.2010.12.018.

Mulla, D.J. (2013). Twenty five years of remote sensing in precision agriculture: Key advances and remaining knowledge gaps. *Biosystems Engineering, 114*(4), 358-371. doi:10.1016/j.biosystemseng.2012.08.009.

Panda, S.S., Hoogenboom, G., Paz, J.O. (2010). Remote Sensing and Geospatial Technological Applications for Site-specific Management of Fruit and Nut Crops: A Review. *Remote Sensing*, *2*(8), 1973–1997. doi:10.3390/rs2081973.

Plant, R.E. (2001). Site-specific management: the application of information technology to crop production. *Computers and Electronics in Agriculture*, *30*(1-3), 9–29. doi:10.1016/S0168-1699(00)00152-6.

Richards, J.A. (1984). Thematic mapping from multitemporal image data using the principal component transformation. *Remote Sensing of Environment, 16*, 35–46.

Robert, P. (1993). Characterization of soil conditions at the field level for soil specific management. *Geoderma, 60*, 57–72.

Schowengerdt, R.A. (2007). Remote sensing: Models and methods for image processing. 3rd ed., Academic Press, San Diego. p. 515.

Schwertmann, U. (1993). Relations between iron oxides, soil color, and soil information. In: Bigham, J.M., Ciolcosz, E.J. (Eds.). Soil Colors. SSSA, Madison, p. 51-69.

Singh, A., Harrison, A. (1985). Standardized principal components. *International Journal of Remote Sensing, 6*(6), 883-896. http://dx.doi.org/10.1080/01431168508948511.

Singh, D., Herlin, I., Berroir, J.P., Silva, E.F., Simoes Meirelles, M. (2004). An approach to correlate NDVI with soil colour for erosion process using NOAA/AVHRR data. *Advances in Space Research*, *33*(3), 328–332. doi:10.1016/S0273-1177(03)00468-X.

Smith L.I. (2002). A tutorial on principal components analysis. Cornell University, USA. p. 27.

Sommer, M., Wehrhan, M., Zipprich, M., Weller, U. (2003). Hierarchical data fusion for mapping soil units at field scale, *Geoderma, 112*, 179–196.

Spielvogel, S., Knicker, H., Kögel-Knabner, I. (2004). Soil organic matter composition and soil lightness. *Journal of Plant Nutrition and Soil Science*, *167*(5), 545–555. doi:10.1002/jpln.200421424.

Statistisches Landesamt Mecklenburg-Vorpommern (Eds.) (2013). Statistisches Jahrbuch. Mecklenburg-Vorpommern, Schwerin, Germany.

Sumfleth, K., Duttmann, R. (2008). Prediction of soil property distribution in paddy soil landscapes using terrain data and satellite information as indicators. *Ecological Indicators, 8*, 485-501.

Triantafilis, J., Gibbs, I., Earl, N. (2013). Digital soil pattern recognition in the lower Namoi valley using numerical clustering of gamma-ray spectrometry data. *Geoderma, 192*, 407-421.

Viscarra Rossel, R.A., Minasny, B., Roudier, P., McBratney, A.B. (2006). Colour space models for soil science. *Geoderma*, *133*(3-4), 320–337. doi:10.1016/j.geoderma.2005.07.017.

Viscarra Rossel, R.A., Cattle, S.R., Ortega, A., Fouad, Y. (2009). In situ measurements of soil colour, mineral composition and clay content by vis–NIR spectroscopy. *Geoderma*, *150*(3-4), 253–266. doi:10.1016/j.geoderma.2009.01.025.

Yan, L., Zhou, S., Feng, L., Hong-Yi, L. (2007). Delineation of site-specific management zones using fuzzy clustering analysis in a coastal saline land. *Computers and Electronics in Agriculture, 56*, 174–186.

Zhang, N., Wang, M., Wang, N. (2002). Precision agriculture--a worldwide overview. *Computers and Electronics in Agriculture, 36*, 113-132.

Zentrales Geologisches Institut (Eds.) (1942). Geologische Oberflächenkarte 1:100.000 (OK100) - 21 Demmin. Berlin.

Zhu, Q., Lin, H.S., Doolittle, J.A. (2013). Functional soil mapping for site-specific soil moisture and crop yield management. *Geoderma*, *200-201*, 45–54. doi:10.1016/j.geoderma.2013.02.001.